Sleep Medicine 85 (2021) 291–302

Contents lists available at ScienceDirect

Sleep Medicine

journal homepage: www.elsevier.com/locate/sleep

Original Article

Focal limbic sources create the large slow oscillations of the EEG in human deep sleep

Kyle K. Morgan [a], Evan Hathaway [a], Megan Carson [a], Mariano Fernandez-Corazza [a, c], Roma Shusterman [a], Phan Luu [a, b], Don M. Tucker [a, b, *]

[a] Brain Electrophysiology Laboratory Company, Eugene, OR, 97403, USA
[b] University of Oregon, Eugene, OR, 97403, USA
[c] LEICI Instituto de Investigaciones en Electrónica, Control y Procesamiento de Señales, Universidad Nacional de La Plata, CONICET, Argentina

ARTICLE INFO

Article history:
Received 9 March 2021
Received in revised form
19 June 2021
Accepted 13 July 2021
Available online 27 July 2021

Keywords:
Sleep
Memory
Slow oscillations
N3 Sleep
Limbic cortex
Dense-array EEG

ABSTRACT

Background: Initial observations with the human electroencephalogram (EEG) have interpreted slow oscillations (SOs) of the EEG during deep sleep (N3) as reflecting widespread surface-negative traveling waves that originate in frontal regions and propagate across the neocortex. However, mapping SOs with a high-density array shows the simultaneous appearance of posterior positive voltage fields in the EEG at the time of the frontal-negative fields, with the typical inversion point (apparent source) around the temporal lobe.
Methods: Overnight 256-channel EEG recordings were gathered from 10 healthy young adults. Individual head conductivity models were created using each participant's own structural MRI. Source localization of SOs during N3 was then performed.
Results: Electrical source localization models confirmed that these large waves were created by focal discharges within the ventral limbic cortex, including medial temporal and caudal orbitofrontal cortex.
Conclusions: Although the functional neurophysiology of deep sleep involves interactions between limbic and neocortical networks, the large EEG deflections of deep sleep are not created by distributed traveling waves in lateral neocortex but instead by relatively focal limbic discharges.

1. Introduction

The functions of sleep are gradually being understood to include specific neurophysiological mechanisms of memory consolidation (Marshall et al., 2020). The replay of events from daytime learning during sleep is associated with improved retention and integration of memories with past experience [1]. These activities of replay and consolidation appear to be mediated through specific neurophysiological interactions between limbic, neocortical, and thalamic networks [2,3]. Extending the findings from animal studies to human sleep has been advanced both by invasive intracranial recordings in epileptic patients [4] and by non-invasive high-density electroencephalographic (HD EEG) studies in healthy adult subjects [5–7]. In the first human HD EEG studies of sleep, the slow oscillations (SOs) of deep (N3) sleep were described as large negative waves over frontal regions that appeared to travel from frontal neocortex toward posterior regions, as if following major pathways of anatomical connectivity [5].

Invasive recordings in neocortex in several species have shown that the slow oscillations (SOs) of deep sleep are associated with abrupt “down states” of minimal neuronal activity that seem to be important to memory consolidation [8,9]. For human HD EEG, the observation of large negative waves over frontal regions would imply that SOs reflect global inhibitory down states that travel across the neocortex [5], an interpretation that is now widely cited in the literature. However, initial efforts at electrical source localization of the cortical generators suggested the onset of SOs was often in the region of insular cortex [6], rather than in frontal neocortex. Furthermore, intracranial recordings in epileptic patients have shown that neocortical activity associated with human SOs is typically not global, but rather local to specific regions of cortex, with a preponderance of the SO down states restricted to anterior cingulate and medial temporal limbic cortices [4]. These observations are not consistent with the interpretation that human

* Corresponding author. Brain Electrophysiology Laboratory Company, Eugene, OR, 97403, USA.
E-mail address: don.tucker@bel.company (D.M. Tucker).

https://doi.org/10.1016/j.sleep.2021.07.028

SOs involve global down states traveling over broad regions of neocortex.

In recent years, improvements in individual head conductivity modeling have allowed more accurate source localization with HD EEG data. Although accurate estimates of head tissue conductivity for each person's head tissue segmentation are important to construct accurate lead fields, the main advantage of creating individual electromagnetic head models with each subject's MRI is that the convolutions of the cortex are specified for that individual, with the result that each patch of cortex (here ~ 1 cm^2) has a known surface orientation and therefore can be used to constrain the dipolar source model for that patch to a specific orientation. Cortical voltage fields are aligned with cortical columns and therefore well modeled with equivalent dipoles perpendicular to the surface. The lead field (forward model) for each individual describes the projection of each dipole patch (delineated by a small sphere in the center of the patch in Fig. 1 **C**) to all 256 electrodes (Fig. 1 **B**). Specifying the orientation of the dipolar cortical source candidates greatly reduces the ambiguity of the source localization problem.

Nonetheless, the mapping from measured head surface voltages to cortical current dipoles requires inverse mathematics, which are ill-posed without unique solutions. An important advance in this inverse estimation has been made with Bayesian methods, including the Multiple Sparse Priors (MSP) method [10] which we use here. The physical constraint of this method is the requirement that source activity at the prior locations must be relatively smooth in relation to adjacent dipoles. A convention is to describe current outflow as a positive dipolar source and current inflow as a dipolar sink. To improve computational efficiency, the prior constraint of local smoothness is implemented sparsely in the present analysis with 400 local priors distributed over the 2400 cortical dipole patches. The MSP constraint shows good reconstruction of simulated sources, with greater accuracy and focality than conventional methods including LORETA and sLORETA. In initial validation studies, we compared our implementation of the MSP algorithm against LORETA and sLORETA. We found that all 3 of these algorithms yielded similar source solutions. However, MSP provided a much more focal solution compared to LORETA and sLORETA which provided more diffuse and variable solutions [11].

The goal of the present study was to characterize the cortical sources of the typical SOs of N3 sleep so that we could then target them accurately with transcranial electrical stimulation (TES) in future studies. We hypothesized that in all subjects the SOs of N3 sleep would be localized more often to limbic rather than neocortical sources.

2. Materials and methods

2.1. Experimental design and EEG acquisition

To characterize the neural generators of SO fields, we collected 256-channel HD EEG during Non-REM stage 3 (N3) sleep from ten healthy young adults (average age = 24; 6 males, 4 females) and conducted both head surface voltage mapping and electrical source localization. The research protocol was approved by the Institutional Review Board at Oregon Research Institute (ORI), and all subjects consented to participate in a study of brain waves during sleep. In addition, all participants shown in the figures here consented to having their faces included in this publication. Prior to

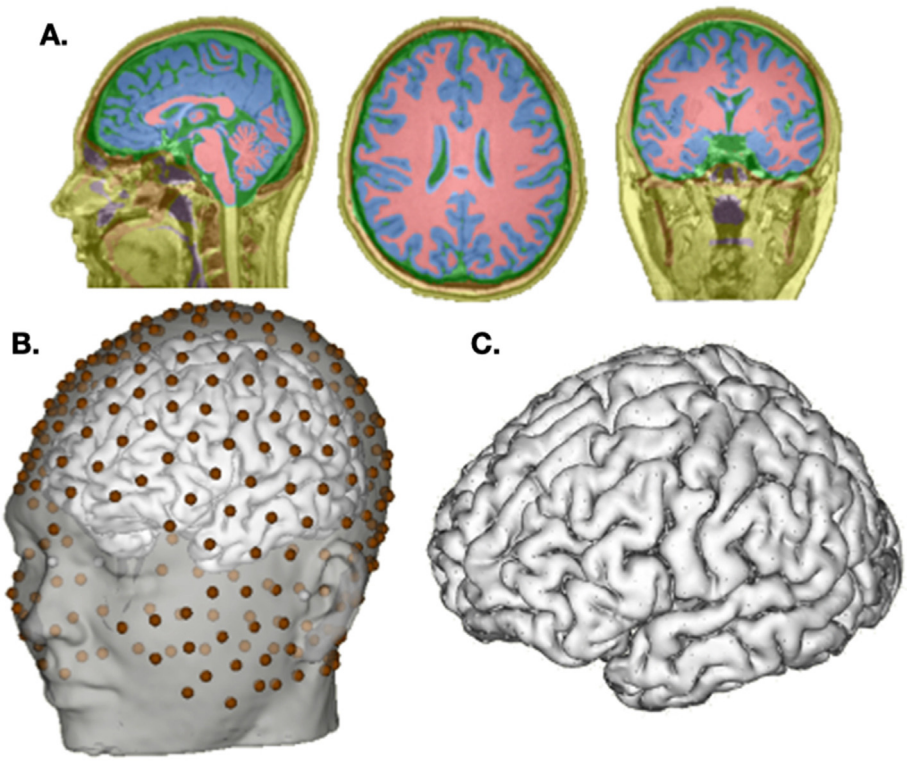

Fig. 1. Electromagnetic head model construction for EEG source analysis. **A:** segmentation of head tissues from T1 MRI, each assigned an appropriate conductivity value (Blue = gray matter, Red = white matter, Orange = bone, Purple = air, Yellow = skin, Green = cerebrospinal fluid). **B:** registration of EEG electrode positions with the head surface on MRI. **C:** This individual's cortical surface, with an equivalent dipole centered on each square cm of cortex surface, oriented normal to the surface to reflect the field pattern for electrical activity at that patch. (For interpretation of the references to color in this figure legend, the reader is referred to the Web version of this article.)

their sleep sessions, a T1-weighted structural MRI was acquired. The T1 included the whole head and neck of each participant to allow modeling of head tissue conductivity. During the sleep session, participants slept in the laboratory typically for 7–8 h in the interval from 10 pm to 7 am. EEG was recorded from 256 channels with the Geodesic Sensor Net, Net Amps amplifiers, and Net Station software (Electrical Geodesics, Inc., Philips Neuro, Eugene, OR USA). Sampling was done at 250 Hz.

2.2. EEG processing and SO identification

DC offsets and high-frequency noise were removed using a 0.1 Hz–40 Hz bandpass filter. To identify SOs of N3 sleep, sleep stages for each EEG recording were determined with a convolutional neural network (CNN). The CNN was trained on the same train, test, and validation datasets as the one described in Ref. [12] and with a similar training schedule. The main differences between the two CNNs are the one used for this study required only three input channels (Left EOG-M2, Right EOG-M1, and M1-M2) and looked back on the 60 s of data preceding the 30-s epoch to be scored.

In this analysis, SOs were defined as large (>75 μV peak-to-peak) slow (0.5–2 Hz) frontal-negative waves. For each subject, SOs meeting these criteria were manually identified and marked at the onset of the frontal-negative peak. To distinguish between SOs and K-complexes of N2, SOs were only marked in epochs scored as N3 by the CNN. In the EEG, SOs have temporal differences between different channel locations, such that an SO recorded from one channel may reach its peak a few milliseconds before the same SO recorded from another channel. This gives SOs the appearance of travelling across the scalp (when the scalp actually reflects only the far field volume conduction). To observe differences in the source localization of SOs with different scalp topographies, we categorized each SO as either left frontal, central frontal, right frontal, left central, central, right central, left temporal, right temporal, both temporal (onset occurring at each hemisphere's lateral temporal locations simultaneously), or occipital based on the scalp location of the channel with the initial onset of the negative peak. The most frequent categories included left or right frontal or central onsets, with a few SOs with apparent temporal or occipital onsets. As some topography categories were more common than others, we marked at least 30 SOs per category for each subject. If there were fewer than 30 SOs in a given category throughout the recording, we marked as many as were present. Once the SO peaks were marked, The EEG was segmented into 2-s windows, centered on each SO peak. The segments were manually evaluated for non-cephalic artifacts (primarily gross movements during sleep, sweating, and channels with poor contact) and artifactual segments were removed. The average number of SOs for each topography category after removing artifactual SO segments, and each category's mean amplitude and range (across subjects) are reported in Table 2. The SOs in each topography category were then averaged, and the average was source localized. SOs are large signal and require minimal (or no) average to have sufficient signal-to-noise ratio for accurate source localization. The main concern, however, is that all SOs included in an average have similar field topography. As a cross-check on the typicality of the average, individual SOs within a topography category were source localized and visually compared to the average.

2.3. Electrical Head Model Construction, Source Analysis, and Statistical Plan

Electrode positions were determined with the Geodesic Photogrammetry System and registered to the individual's MRI [13]. An individual head conductivity model was created for each participant with the *Sourcerer* software (BEL Company, Eugene, OR, USA). For each participant, the structural T1-weighted MRI was segmented into 7 tissue types (scalp, skull, cerebrospinal fluid, gray matter, white matter, internal air, eyeballs) (Fig. 1 **A**). The cortical surface was extracted from the MRI with the marching cubes algorithm and tessellated into 1200 surface patches per hemisphere, with each patch modeled by an equivalent dipole oriented normal to the patch mean surface orientation. Conductivity values were assigned to each tissue type to create a finite element model describing the lead field (conductivities between electrodes and dipoles for each cortical patch). The conductivity values of each tissue were assigned according to literature values: 0.35 S/m for WM [14], 0.01 S/m for the skull [15], 0.33 S/m for the scalp [16], 1.79 S/m for CSF [17], 0.25 S/m for GM [14] and 1.55 S/m for the eyeballs [18]. The completed electromagnetic head model is illustrated in Fig. 1 **A**.

Each subject's brain was registered to MNI space, and the Brodmann area (BA) of each source was determined. Of the 54 Brodmann areas included in our analysis (Fig. 2 **A**), 28 areas were labeled as limbic cortex and 26 as nonlimbic or lateral neocortex (limbic areas are highlighted in the flat map in Fig. 2 **C**). Each topographically different average SO was localized for each subject with the Bayesian MSP algorithm and frequency counts for limbic and nonlimbic neocortical BA categories were totaled. A repeated measures analysis of variance was used to test the statistical significance of differences in limbic versus nonlimbic neocortical localizations of all average SOs for each subject.

3. Results

3.1. Exploratory analysis of SOs

In our initial exploratory analysis, we examined head surface voltage maps for several hundred SOs for ten healthy young adults during deep sleep (Non-REM Stage 3 or N3). SOs are large (~75 μV) frontal-negative deflections that are readily observed in the EEG (Fig. 3 **A**). Although these events are classically described as sinusoidal oscillations at 0.5–2 Hz [19]), and they often occur in a series, careful inspection shows that SOs are transients, with a discrete frontal-negative discharge followed by a smaller (asymmetric and thus non-sinusoidal) frontal-positive following wave (Fig. 3 **A**). We mapped the SO voltage field at the peak of the frontal-negative discharge with a reference-independent method [20]), specifically the average reference computed over the 256 channels shown in Fig. 1 **B**. This simple method of accurate (reference-independent) voltage field mapping showed that the frontal-negative head surface voltage field is balanced by a positive voltage field over the back of the head. Fig. 3 **B** shows the voltage field of a single SO marked in the EEG chart (Fig. 3 **A**). By the first principles of volume-conducted electrical fields [21,22], the neural source generating this field is not defined by the frontal negativity, but by the dipolar inversion of the negative and positive fields. In the SO in Fig. 3 the inversion creates an isopotential line (zero voltage indicating the source of the dipolar generator) over central and mid-temporal regions, with a field pattern that suggests a generator deep in the hemisphere.

To contrast this typical SO voltage field topography with the scalp patterns to be expected by a neocortical traveling wave, we performed a simulation in which an individual's head conductivity model was used to accurately map the surface fields of dipolar sources placed in dorsolateral frontal cortex (Fig. 4 **A**, **B**, and **C**). The forward projection (from cortex to scalp) of the dipolar source describes what a surface field would look like if the source of an SO were truly frontal. In Fig. 4 **A**, sources were placed slightly more anteriorly, in Fig. 4 **B** they were midway, and Fig. 4 **C** they were placed more posteriorly, to illustrate how a traveling cortical-surface-negative wave would appear at the head surface. Note that, as expected for a source in the superior neocortex, the voltage

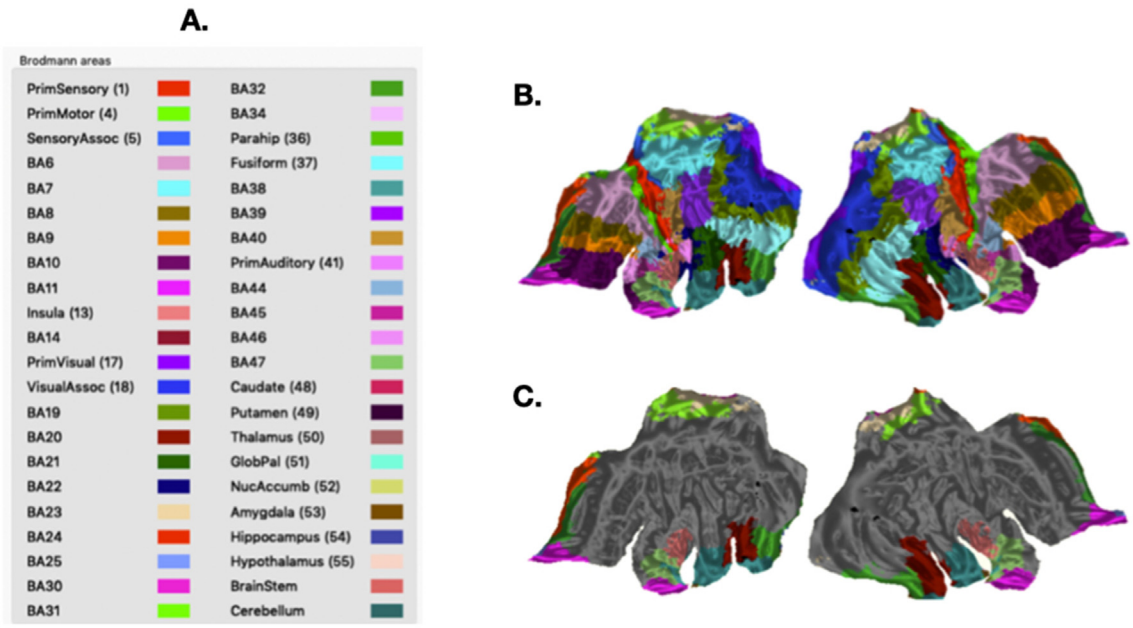

Fig. 2. **A:** The legend identifies each BA with a unique color. **B:** A parcellated flat map showing the boundaries of each Brodmann area. **C:** The BAs that were designated as limbic. (For interpretation of the references to color in this figure legend, the reader is referred to the Web version of this article.)

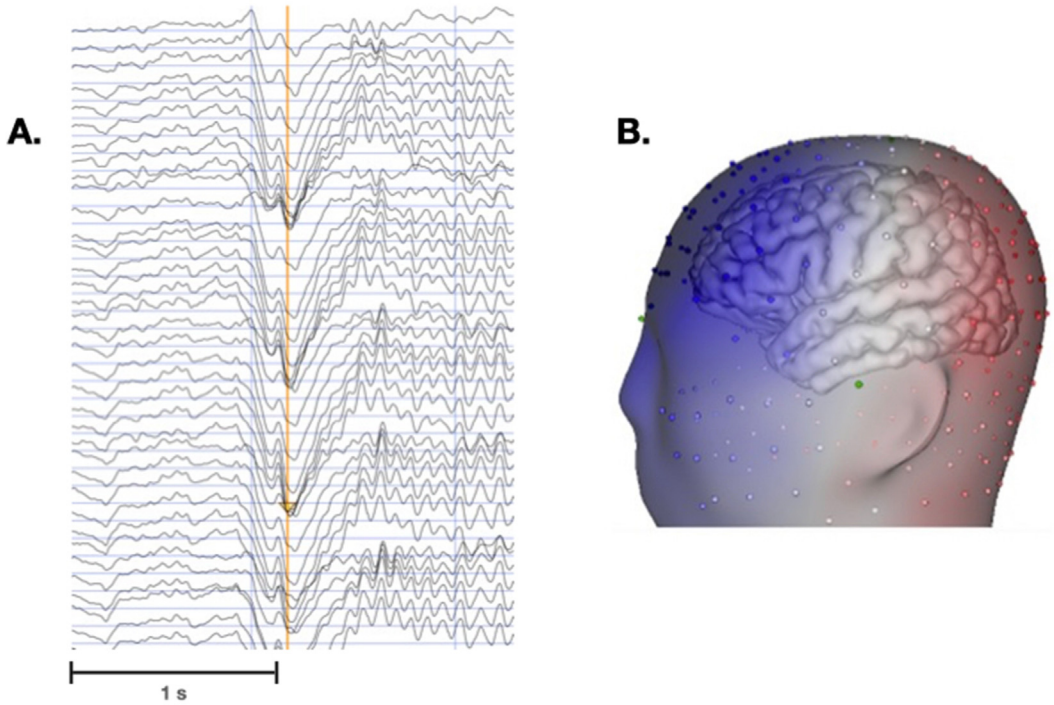

Fig. 3. A typical SO in N3 sleep of a healthy young adult. **A:** Chart view of 40 frontal channels of EEG showing the SO (marked with brown vertical line) as a surface-negative frontal discharge. **B:** the head surface distribution of the EEG potential fields (average reference) plotted in relation to the electrode locations on an atlas head model (blue = negative voltage field; red = positive field; white = zero potential). (For interpretation of the references to color in this figure legend, the reader is referred to the Web version of this article.)

inversion line (white) is also near the superior head surface. In contrast, a SO actually recorded from this person (Fig. 4 **D**) shows a similar frontal negativity, yet the whole head surface field (mapped with a reference-independent method) shows the dipolar inversion is at the middle (equator) of the head, with the matched positive field distributed over the back of the head, consistent with a source deep in the head (such as in limbic cortex). Guided by the principles of volume conduction illustrated in Fig. 4, the present study was conducted to characterize the typical head surface voltage topographies of SOs in deep (N3) sleep, and to localize the neural sources that could account for these topographies.

The CNN for scoring sleep stages in the present study achieved similar accuracy as the one used in Ref. [12] when predicting the human scoring of the test set, with F1 = 71, acc = 82 %, and

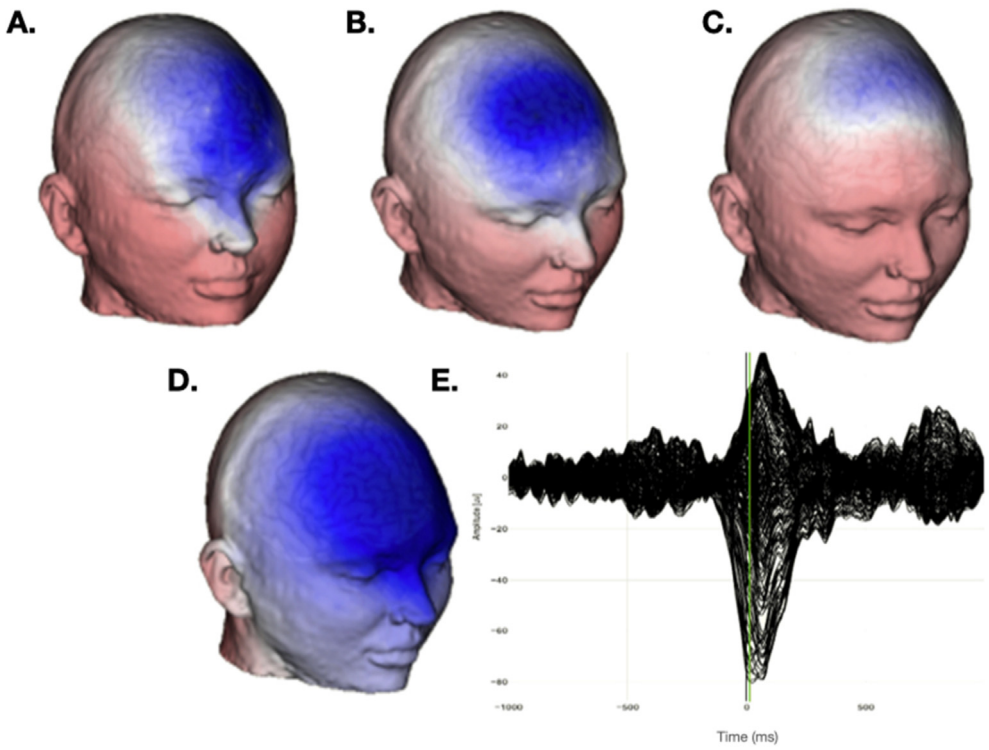

Fig. 4. Top: Simulations of dorsolateral frontal cortical dipolar sources with frontal-negative fields, with more anterior **(A)** and slightly more posterior (**B** and **C**) frontal cortex locations, as might be seen with a superficial nonlimbic neocortical traveling wave. Note the inversion lines are close to the sources, consistent with the field patterns of superficial cortical sources. **Bottom:** Actual 256-channel recording of a single (not averaged) slow oscillation (SO) of deep sleep for this person, showing the head surface voltage topography (**D**). The source explaining this field pattern could not be superficial frontal cortex. **E:** The butterfly plot, with all channels overplotted, indicating the time of this field map (green line) just before the peak of this large frontal-negative voltage deflection. (For interpretation of the references to color in this figure legend, the reader is referred to the Web version of this article.)

Table 1
Time (minutes) spent in each stage of sleep for the ten subjects.

Subject	Total Time	Wake	N1	N2	N3	REM
1	506.0	52.5	10.5	200.5	128.0	114.5
2	482.0	25.5	62.0	206.0	97.0	91.5
3	489.5	30.5	159.5	42.0	80.0	177.5
4	515.5	95.0	17.0	255.0	63.0	85.5
5	529.0	44.0	48.5	174.0	155.0	107.5
6	496.5	71.5	23.5	128.0	129.5	144.0
7	524.0	91.0	49.0	176.5	114.0	93.5
8	542.0	267.5	22.5	79.5	81.5	91.0
9	488.5	54.0	30.0	163.0	155.5	86.0
10	498.5	17.5	20.0	205.0	116.0	140.0

kappa = 0.74. In Table 1 we report time spent in each stage of sleep for each subject.

Table 2 shows the number of artifact-free SOs in each topography category, the negative amplitude (negative deflection) for the average for that category, and the values for the smallest and largest SOs in that category. For frontal and central peak onset categories, the individual SO localizations were consistent with the averages upon inspection. However, the individual SOs had more noise and were more variable in their localization; the SOs of temporal lobe clusters (infrequently observed as shown in Table 2) were more variable within the cluster, such that the representativeness of the averages was also more variable in those small category clusters.

3.2. Source analysis of SOs from individual subjects

All SO averages for all subjects were analyzed and quantified (section 3.3); the figures in the present section were generated using selected SO averages from a few subjects to illustrate typical patterns observed in individuals, each based on the individual's MRI to characterize both head tissue conductivity and cortical surface geometry. Fig. 5 shows the head surface voltage measurements and the source localization of a cluster of one subject's SOs with initial EEG surface topography appearing in the central frontal region of the head. The average-referenced EEG waveforms in the chart view of 40 frontal channels (Fig. 5 **i.**) show the typical pattern of a strong frontal-negative deflection followed by a smaller frontal-positive wave. The head surface voltage map shows that the frontal-negative peak of the SO is balanced by a corresponding posterior-inferior positivity (**ii.**). Source localization of this person's central-frontal onset SO average with the Bayesian Multiple Sparse Priors (MSP) solution (**iii**, **v**, with cortical flat maps shown in **vii**) shows the frontal negativity is explained by a right-lateralized orbitofrontal cortical source (cortical surface current outflow, here shown in red), together with smaller sinks in anterior medial temporal sites (blue). An alternative source inversion (sLORETA) is shown for the ventral brain surface (**vii**) and for the flat maps (**viii**). As is typical in our experience, the Bayesian MSP solution is more focal and more stable in the presence of noise than the sLORETA (or LORETA) inverse solutions. A legend with Brodmann Areas for the flat maps, and a delineation of limbic areas, are shown in Fig. 2.

The smaller following positive wave for this SO average is shown in Fig. 6, with the time point for the head surface map and cortical source localization marked by the brown vertical line in both chart (**i**) and butterfly plots (**iv**). Consistent with the inversion of the head surface voltage field from frontal-negative SO to frontal-positive following wave, the right orbitofrontal source for the SO inverts for the positive following wave to a cortical sink

Table 2
SO characteristics by topographical category. Means and standard deviations are computed across all subjects. For each topographical category we provide means and standard deviations for (1) the number of artifact-free individual SOs identified, (2) the most negative deflection of the averaged SO waveform, (3) the most negative deflection of the smallest individual SO waveform, (4) the most negative deflection of the largest individual SO waveform. The most negative deflection of each SO waveform was calculated by taking the most negative value across all samples and channels in a 2-s window centered around the negative peak. This is different than the peak-to-peak difference between the most negative and most positive amplitude values.

Topographical Category	Number of Artifact-free SOs		Negative Deflection of Averaged SO (μV)		Negative Deflection of Smallest SO (μV)		Negative Deflection of Largest SO (μV)	
	Mean	SD	Mean	SD	Mean	SD	Mean	SD
Left Frontal	10.15	3.67	−95.40	30.27	−77.23	18.94	−238.15	85.46
Central Frontal	8.23	3.35	−96.27	15.27	−80.66	33.06	−206.52	42.17
Right Frontal	9.00	3.87	−95.20	29.19	−84.46	30.08	−206.41	69.18
Left Central	10.00	4.12	−96.06	26.66	−76.92	31.29	−209.63	46.16
Central	11.31	4.55	−113.64	40.42	−79.80	25.02	−249.53	91.08
Right Central	9.23	3.17	−103.62	35.39	−86.56	38.25	−212.10	45.58
Left Temporal	1.69	3.57	−60.46	16.15	−74.66	8.74	−150.89	58.89
Right Temporal	0.69	1.97	−71.24	39.74	−77.97	18.94	−189.90	3.89
Both Temporal	1.00	2.52	−86.04	30.22	−98.75	24.48	−139.76	17.06
Occipital	0.62	1.50	−82.53	10.65	−65.59	8.51	−152.64	24.73

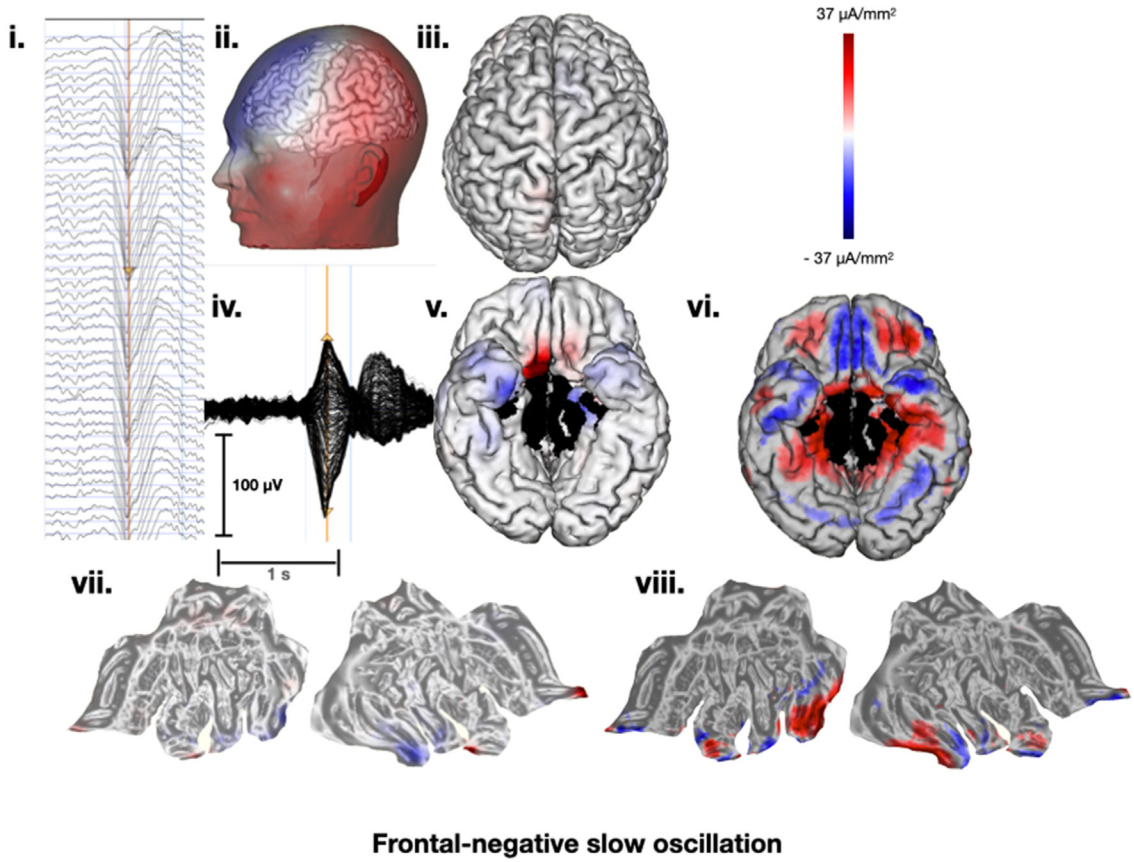

Fig. 5. Localizing a typical SO average with central frontal onset from a young adult at the frontal-negative peak. **i.** negative deflection of the large SO in 40 frontal EEG channels. **ii.** Head surface voltage at the SO peak. **iii.** Dorsal view of cortical activations at this peak. **iv.** Butterfly plot of this subject's average central frontal SO with marker at the SO peak. **v.** Ventral view of cortical activations with Bayesian multiple sparse priors (MSP). A focal current source (cortical current outflow) in right orbital cortex, along with a right basal temporal pole sink. **vi.** Localizing the same time point with sLORETA inverse. **vii.** MSP solution showing orbital cortical sources (red) and medial anterior temporal sinks (current inflow, blue) shown on the cortex flat map, for which the cortical surface is unfolded to a 2D surface. **viii.** flat map display for the sLORETA inverse solution. This layout is used for other source localization figures. (For interpretation of the references to color in this figure legend, the reader is referred to the Web version of this article.)

(blue spot in the ventral brain surface) in the MSP solution (Fig. 6 **v** &**vii**). The anterior medial temporal sinks of the SO also invert in the following wave, to cortical sources. This stereotyped electrophysiological progression is typical for SOs we examined and suggests the SO voltage field in the EEG slow wave of deep sleep is generated by the limbic cortex site [23], which for this example is primarily right caudal orbitofrontal. A more diffuse pattern of results is seen for the sLORETA solution in the ventral brain image (Fig. 6 **vi**) and flat maps (**vii** & **viii**). The spread of the sLORETA solution appears to reflect the smaller signal-to-noise ratio of this

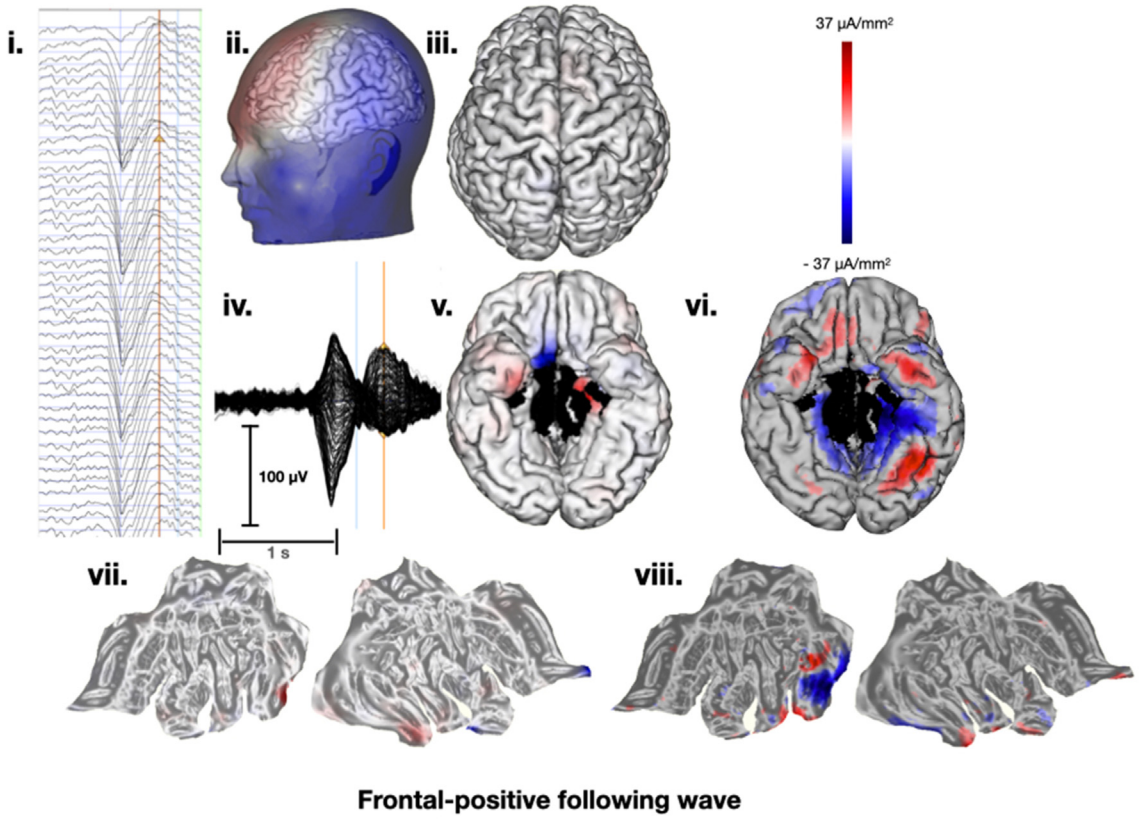

Fig. 6. Source localization for the positive following wave for the SO in Fig. 5. In both the MSP and sLORETA inverses, the positive following wave of the SO shows an inversion of cortical current sources and sinks. **i.** positive deflection following the large SO in 40 frontal EEG channels. **ii.** Head surface voltage at the positive peak. **iii.** Dorsal view of cortical activations at this peak. **iv.** Butterfly plot with marker at the following positive peak. **v.** Ventral view of cortical activations with Bayesian multiple sparse priors (MSP). **vi.** Localizing the same time point with sLORETA inverse. **vii.** The flat map view of the MSP source localization **viii.** Flat map display for the sLORETA inverse solution.

small following wave, compared to the strong signal of the negative-going SO itself.

In order to provide convergent validation for the fit of the focal source model for this subject's frontal-negative SO in Fig. 5, we simulated a single current dipole in the right caudal orbital cortex of this subject's electromagnetic head model, at the approximate location of the primary source (red spot) in Fig. 5 **v**, ignoring the smaller activations. The head surface (forward) projection from this focal dipolar source is shown in Fig. 7 **A**. The comparison of this simulation with the subject's actual voltage field at this time point (Fig. 7 **B**) shows a reasonable reconstruction of the head surface voltage field for this focal source model of the frontal-negative SO. This field pattern, with an inversion line over temporal and caudal orbitofrontal cortex, is typical for the majority of the SOs we observed in this sample of subjects.

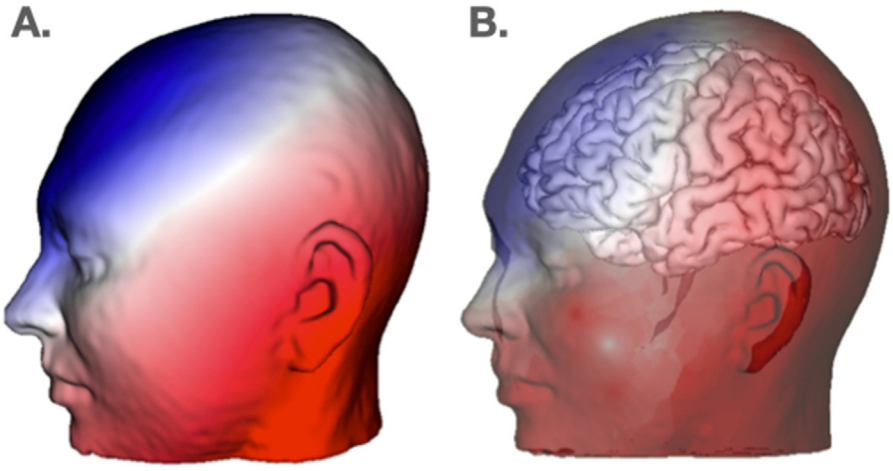

Fig. 7. A: The forward projection of the voltage field that would be created by a single source in the right caudal orbital region, consistent with the primary localization of the frontal-negative SO in Fig. 5. This head surface field generally matches the actual EEG voltage field from this SO average (**B**). The differences in the head surface field are created by the additional cortical activity in the actual data, including the temporal pole sinks seen in Fig. 5.

Figure 8 shows another SO average for this subject (the same person as in Figs. 5–7), with the frontal-negative wave for this topographic cluster (Fig. 8 **A**) showing a somewhat right-lateralized onset. This field pattern is created by a left caudal orbital source (red spot in the ventral brain view), which inverts to a sink for the positive following wave (Fig. 8 **B**).

Figure 9 illustrates a typical frontal-negative SO average for another subject, and Fig. 10 shows the frontal-positive following wave for this SO. The frontal-negative head surface field (Fig. 9) was somewhat superficial for this SO cluster. The MSP source analysis indicated a source in the left anterior medial temporal area, a sink in the left basal temporal pole, and a left anterior cingulate sink (seen in the flat map, Fig. 9 **vii.**). Based on experience with forward field modeling (for example, Figs. 4 and 7), the somewhat superficial field inversion for this frontal-negative SO seems to have been created by the left anterior cingulate sink (closer to the head surface than the typical medial temporal and orbital sources). The frontal-positive following wave of this average (Fig. 10) was not well synchronized with the average SO as can be seen in the butterfly plot (perhaps because of timing variability over epochs in the average) and as a result was noisy. However, the MSP source analysis still suggested an inversion of the left basal temporal sink (to a source). This inversion was not so clear in the sLORETA inverse, which again seems to have been indeterminant in the presence of noise compared to the MSP inverse.

Figure 11 shows an SO average from another subject, with the typical frontal-negative (posterior-positive) surface topography shown in **A**. This time the MSP results showed a source-sink inversion in the right anterior medial temporal lobe, apparently dividing the parahippocampal gyrus. Although the following frontal-positive wave shown in Fig. 11 **B** is small, diffuse, and variable, there are suggestions of inversions of the SO sources, including for the right parahippocampal area and several basal regions of the left hemisphere.

3.3. Statistical summary of SO localizations to limbic and nonlimbic cortex

We conducted a quantitative summary of all of the SO localizations, with statistical contrasts between limbic and nonlimbic Brodmann areas, for this sample of subjects. For each person's N3 SOs, a count of the primary localization of the SO average for each of their topographic SO clusters were made for each Brodmann area, and these localization counts were then summed over the 10 participants. The statistical contrast was between SO counts in the limbic versus neocortical Brodmann areas included in our analysis: 28 areas were counted as limbic cortex (Fig. 12**A**) and 26 were counted as nonlimbic neocortical. On average, slow oscillations (SOs) were localized to 20.1 limbic areas per subject (SD = 8.17), whereas sources in the nonlimbic neocortex (covering a substantially larger cortical surface area) were observed in 9.6 Brodmann areas per subject (SD = 7.57). A paired-samples t-test revealed that limbic sources were significantly more frequent than neocortical sources ($t(9) = 3.922$, $p = 0.003$). Figure 12 **B** presents the histogram of these total counts over Brodmann areas in the bottom set of flat maps, showing the high frequency of ventral limbic (medial temporal and orbitofrontal) localizations, and the lower frequency of dorsal limbic generators (excepting the anterior cingulate cortex on the left). Remarkably, these SO discharges were considerably more frequent for left than right limbic regions. The only neocortical area with frequent SOs was the left fusiform area.

4. Discussion

EEG source localization with ten young adults showed that the large frontal-negative deflections of slow oscillations (SOs) in human deep sleep are typically explained not by a global neocortical traveling wave but by focal activity in limbic cortex. SOs, conventionally defined as greater than 75 μV, are the largest voltage fluctuations observed in

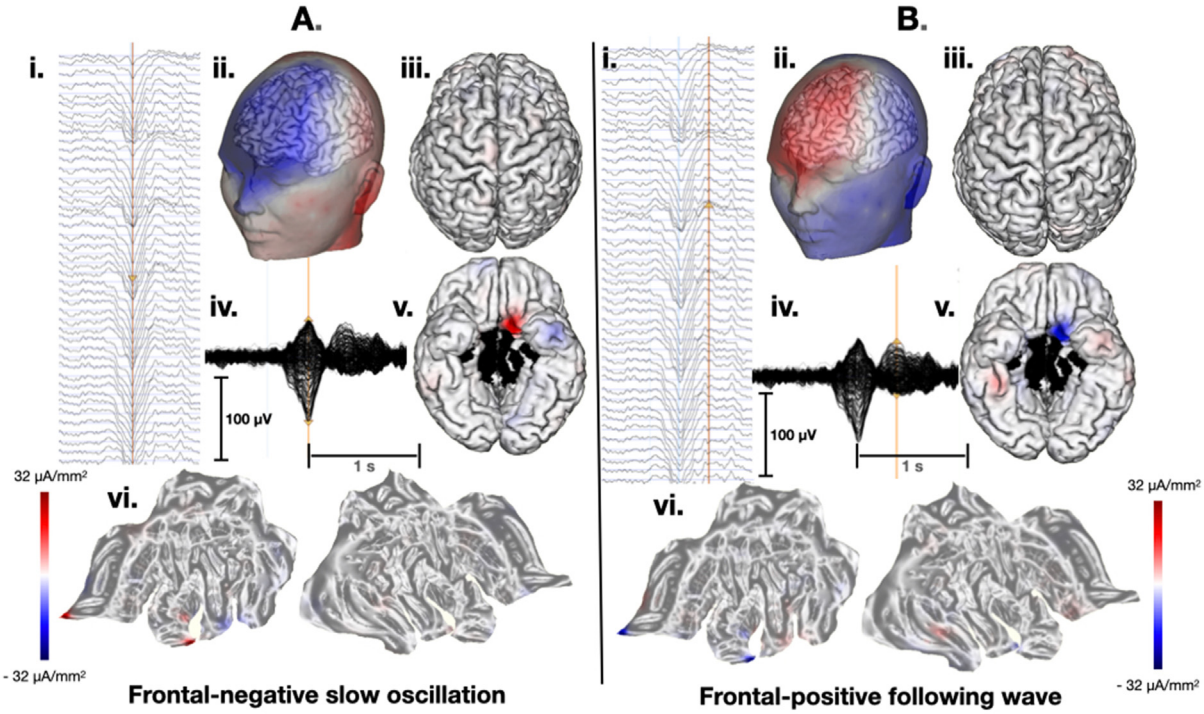

Fig. 8. A: A different SO for the subject shown in Figs. 5 and 6, with MSP inverse, with a somewhat right-lateralized frontal-negative wave described primarily by a left caudal orbital frontal source. **B**: The following positive wave for this SO, showing an inversion of the SO negative phase to a caudal orbital frontal sink.

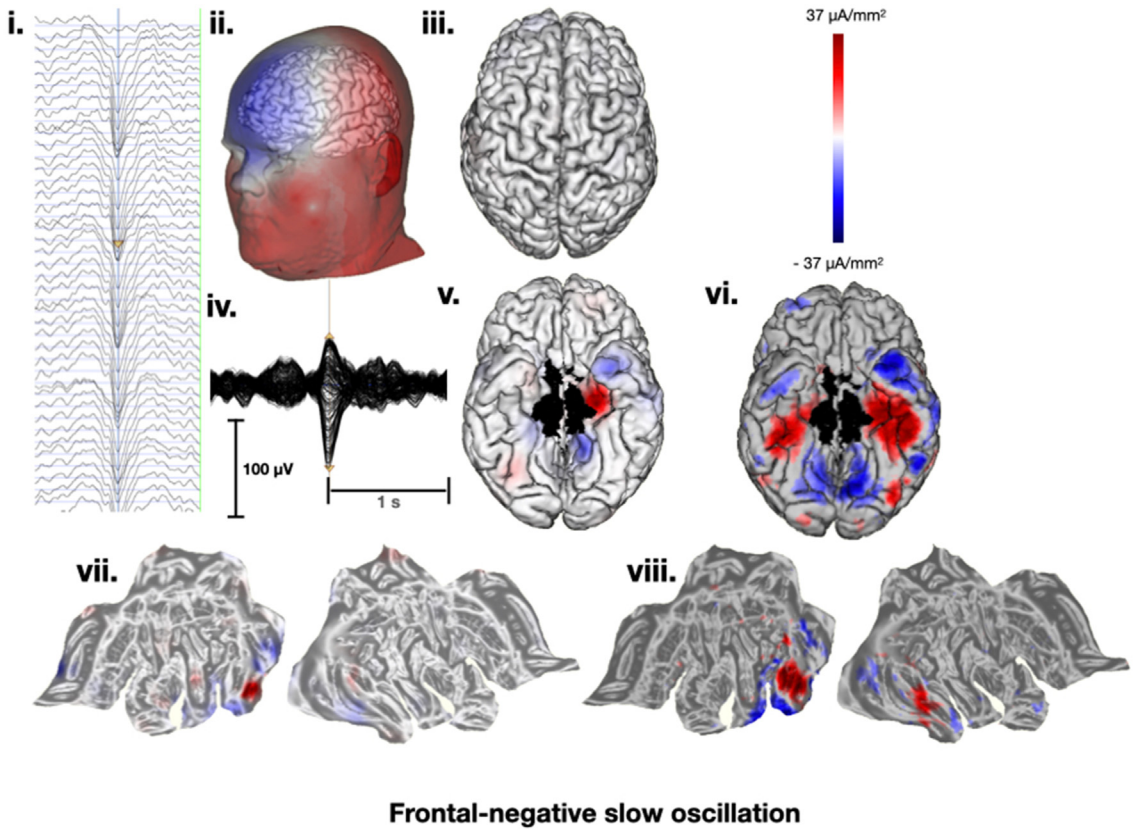

Fig. 9. Source localization for a frontal-negative SO for a different person (not from Figs. 5, 6 and 8) showing a left medial temporal cortical source and adjacent sinks in the MSP solution (**v.** & **vii.**) and a similar (but more diffuse) localization with sLORETA (**vi.** & **viii.**).

the EEG of healthy persons. The finding that SOs emanate primarily from regions of limbic cortex implies that these limbic regions not only generate the large voltage fields of the EEG, but that they also contribute in some way to the neurophysiology of cortical down states associated with memory consolidation. Given the importance of limbic–neocortical interactions in sleep [2,3,8], further research on the relation between limbic generation of SOs and the down states of the neocortex may provide insight into the specific mechanisms of memory consolidation.

The functional role of SOs in human N3 sleep in memory consolidation has been suggested by several lines of evidence, including the impaired N3 sleep in older persons with impaired memory [24], and the improvement of declarative memory when electrical stimulation is applied to induce and synchronize SOs during sleep [25]. Practically, accurately characterizing the neural sources of SOs may allow more effective targeting with transcranial electrical stimulation (TES) to improve deep sleep. Previous efforts to enhance sleep with SO synchronization [25,26] have targeted the frontal lobes generally. However, the present results suggest that electrical synchronization may be more effective if directed to orbitofrontal and anterior medial temporal sites specifically. A recent test of this proposal in our laboratory [12] confirmed that the SOs of N3 sleep could be enhanced by targeting anterior ventral limbic areas specifically, using half the current (0.5 mA vs 1.0 mA) of previous studies.

The Bayesian Multiple Sparse Prior algorithm for inverse source reconstruction is constrained by smoothness on the local cortical surface [10], and thus suited to reconstruct focal sources. Nonetheless, a limbic source at a medial site deep in the cerebral hemisphere was indicated for most SOs not only by more conventional source reconstructions (LORETA, sLORETA), but also by forward modeling from possible electrical source generators (Figs. 4 and 7). Side-by-side contrasts of the Bayesian Multiple Sparse Prior results with sLORETA were also examined in Ref. [11]. Similarly, in the present results, sLORETA and LORETA showed comparable localization of the SO cortical focus, but with a more distributed (diffuse) pattern. The most frequent localizations of SOs in the present study were to the anterior medial temporal lobe and the orbital frontal lobe. These ventral limbic localizations were more frequent on the left side, consistent with previous findings of left lateralization of human SOs [27].

Because our cortical surface extraction methods followed the cortical surface to the limbic boundary of the medial hemisphere, the geometric characterization of the uncus and anterior parahippocampal gyrus was approximate in many cases. Better cortical surface geometry, careful attention to exact electrode positions, and likely greater density of EEG sampling will be required for more precise localization of SOs to the specific entorhinal and piriform cortices of this area.

Even with this somewhat rough localization, the present results indicated that the large SOs of N3 sleep originate most frequently in anterior medial temporal lobe, and secondarily in caudal orbitofrontal lobe. A basic question is how this activity of limbic cortex relates to the activity of nonlimbic neocortex (heteromodal and unimodal association areas and primary sensorimotor areas). Several lines of evidence show that the neocortex includes inherent

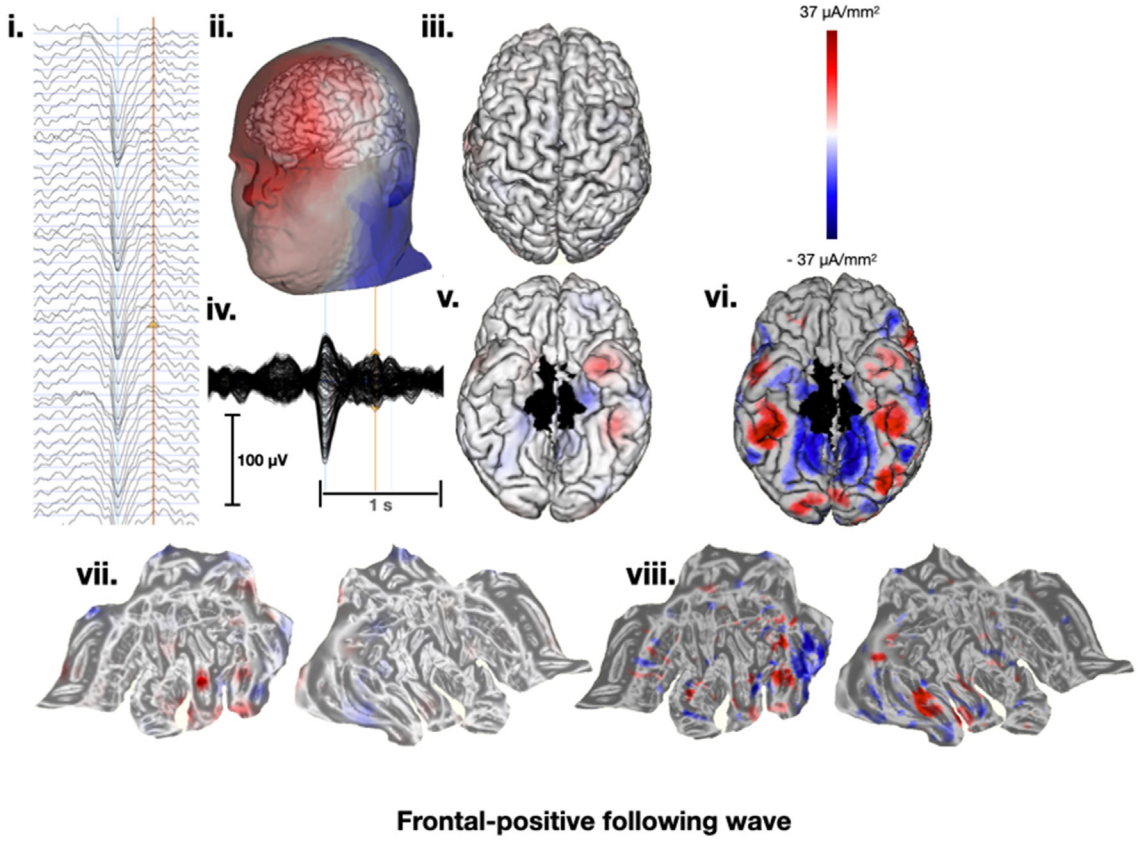

Fig. 10. Source localization for the frontal-positive following wave for the same person in Fig. 9. The inversion of the left medial source to a sink is clear in the MSP solution (left) but not so clear in the sLORETA solution (**vi.** & **viii.**). Note that this following wave is complex and low amplitude, possibly explaining the less clear source localization results.

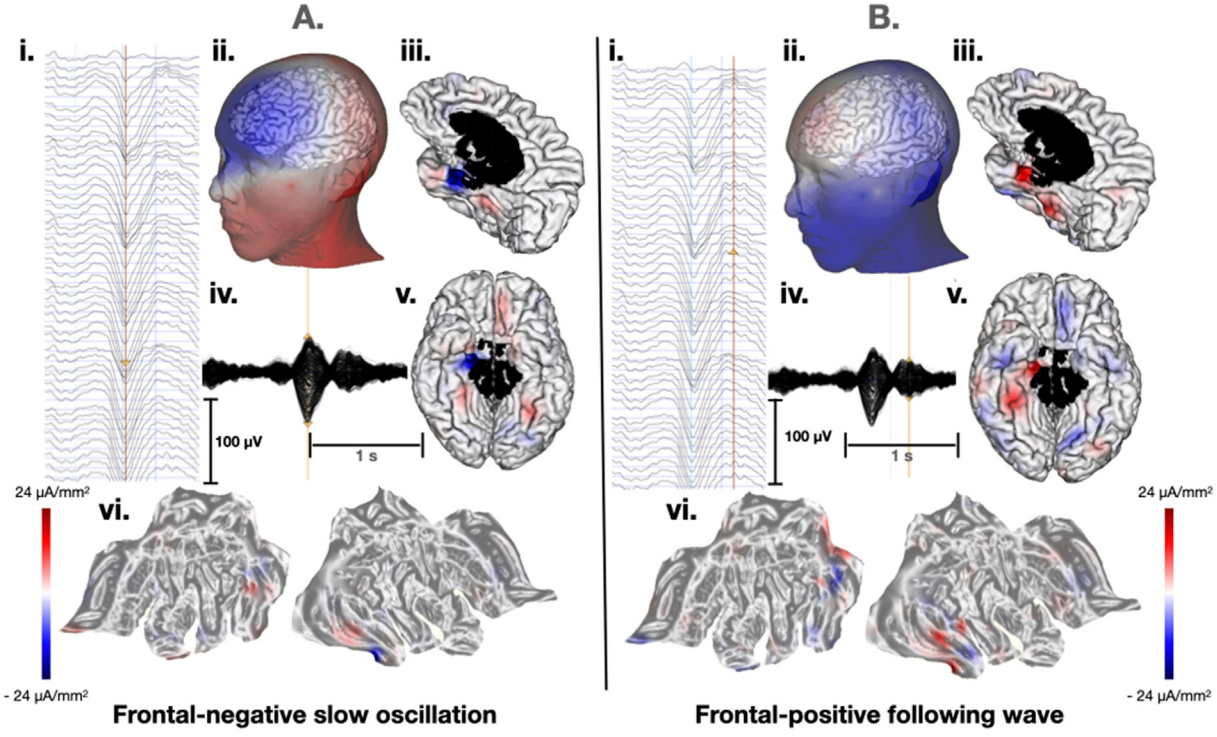

Fig. 11. Source model (MSP) for a frontal-negative SO average **(A)** with a dominant sink/source distribution in the right medial temporal area and an inversion of this pattern for the frontal-positive following wave (**B**).

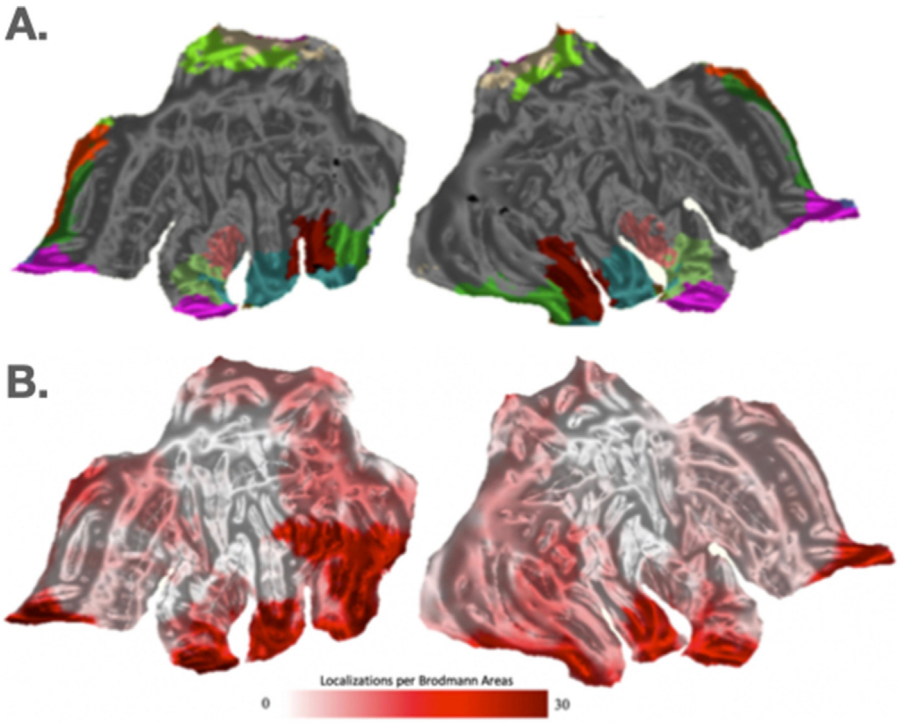

Fig. 12. A: The BAs we designated as limbic. **B:** A histogram of counts of frontal-negative SO localizations during N3 sleep in each Brodmann area for the ten adults, showing that most SOs are generated in ventral limbic (anterior medial temporal and caudal orbitofrontal) areas, particularly on the left side.

mechanisms for generating slow oscillations, and that these intrinsic neocortical circuits are important to the regulation and propagation of local down states [28].

It is significant that the majority of the SOs of N3 sleep for these subjects were generated not just by limbic cortex, but more specifically by *ventral* limbic cortex (paleocortex), including anterior medial temporal (parahippocampal gyrus and temporal pole) and caudal orbital cortex. The paleocortical base of the ventral division of the hemisphere contrasts with the archicortical base of the dorsal corticolimbic division that includes the hippocampus and cingulate cortex [29–32]. Although we observed a number of SOs partially explained by left anterior cingulate sources, the anterior cingulate cortex is unique in the dorsal brain by having considerable ventral limbic connectivity through the subgenual caudal orbital region [33,34].

Related to this ventral limbic preponderance of SO discharges, recent optogenetic studies in mice have shown that the claustrum regulates both SOs and the associated GABAergic inhibitory control of neuronal activity in neocortical down states [35]. Although the claustrum has widespread limbic and medial frontal projections [36], several lines of evidence suggest it is preferentially connected with the ventral limbic base of the hemisphere [37]. In the recent Narikiyo findings, the claustrum projections in mice were particularly dense with ventral limbic areas including the insular and orbital cortex (Fig. 2 of Narikiyo et al., [35]. In mice with a Pax-6 mutation that disrupts the embryonic differentiation of the claustrum, the ventral limbic division of the cortex is specifically disrupted, whereas the dorsal limbic division develops normally [38]. If there is a ventral limbic (and therefore ventral neocortex) specificity of SO regulation of cortical inhibitory down states, there may be important implications for understanding the unique mechanisms of memory consolidation in deep N3 sleep.

In contrast, recent EEG source localization of slow and sawtooth waves in REM sleep has suggested a dorsal limbic (cingulate) source [39]. Contrasting the limbic networks engaged in REM with those engaged in N3 sleep may suggest that paleocortical and archicortical regions of the limbic system consolidate their associated networks of ventral and dorsal neocortex through their specific connectivity, achieving unique forms of memory through the markedly differing neurophysiologic mechanisms of deep sleep and REM sleep, respectively.

Although further progress with HD EEG source localization can be expected to clarify the specific interactions between limbic and neocortical networks, an important near-term strategy will be to combine HD EEG at the head surface with intracranial recordings (icEEG), such as are conducted in evaluating epileptic patients. Intracranial recordings in epileptic patients have revealed local patterns of down and up states in cortex [4,40], with a preponderance of limbic (medial temporal and anterior cingulate) sources shown by Nir et al. that may parallel the present results. Although a selective sampling of regional cortical activity is inherent to the clinical placement of electrodes in intracranial recording of epileptic patients, and intracranial recordings are limited to resolving only local cortical activity, the whole head mapping of field patterns of SOs with HD EEG can characterize the full patterns of network function that are related to regional up and down states. Combining HD EEG and icEEG could therefore provide novel theoretical insight into the corticolimbic neurophysiology of memory consolidation.

Credit Author Statement

Kyle Morgan: Formal Analysis, Methodology, Investigation, Writing – Original Draft, Writing – Review & Editing, Visualization Evan Hathaway: Methodology, Software, Formal Analysis, Investigation, Writing – Original Draft, Writing – Review & Editing, Visualization Megan Carson: Methodology, Investigation, Resources, Writing – Review & Editing, Supervision Mariano Fernandez-Corazza: Methodology, Software Roma Shusterman: Conceptualization Phan Luu: Conceptualization, Methodology,

Software, Visualization Don M. Tucker: Conceptualization, Methodology, Writing – Original Draft, Writing – Review & Editing, Project Administration, Funding Acquisition.

Acknowledgements

This research was supported by National Institute of Mental Health Small Business Innovation Research grant R44MH115955.

Conflict of interest

The authors are employees and contractors of The Brain Electrophysiology Laboratory Company, a developer of commercial neuromonitoring and neuromodulation technologies.

The ICMJE Uniform Disclosure Form for Potential Conflicts of Interest associated with this article can be viewed by clicking on the following link: https://doi.org/10.1016/j.sleep.2021.07.028

References

[1] Walker M. Why we sleep: unlocking the power of sleep and dreams. New York: Scribner; 2017.
[2] Buzsáki G. Hippocampal sharp wave-ripple: a cognitive biomarker for episodic memory and planning. Hippocampus 2015;25(15):1073–188.
[3] Crunelli V, David F, Lőrincz ML, et al. The thalamocortical network as a single slow wave-generating unit. Curr Opin Neurobiol 2015;31:72–80.
[4] Nir Y, Staba RJ, Andrillon T, et al. Regional slow waves and spindles in human sleep. Neuron 2011;70(1):153–69.
[5] Massimini M, Huber R, Ferrarelli F, et al. The sleep slow oscillation as a traveling wave. J Neurosci 2004;24(31):6862–70.
[6] Murphy M, Riedner BA, Huber R, et al. Source modeling sleep slow waves. Proc Natl Acad Sci U S A 2009;106(5):1608–13. https://doi.org/10.1073/pnas.0807933106.
[7] Riedner BA, Vyazovskiy VV, Huber R, et al. Sleep homeostasis and cortical synchronization: III. A high-density EEG study of sleep slow waves in humans. Sleep 2007;30(12):1643–57. Retrieved from, http://www.ncbi.nlm.nih.gov/pubmed/18246974.
[8] Buzáki G. The hippocampal-neocortical dialogue. Cerebr Cortex 1996;6:81–92.
[9] Todorova R, Zugaro M. Isolated cortical computations during delta waves support memory consolidation. Science 2019;366(6463):377–81.
[10] Friston K, Harrison L, Daunizeau J, et al. Multiple sparse priors for the M/EEG inverse problem. Neuroimage 2008;39(3):1104–20.
[11] Fernandez-Corazza M, Feng R, Ma C, et al. Source localization of epileptic spikes using Multiple Sparse Priors. Clin Neurophysiol 2021;132(2):586–97.
[12] Hathaway E, Morgan K, Carson M, et al. Transcranial electrical synchronization targeting limbic cortex increases the duration of human deep sleep. Sleep Med 2021;81:350–7. https://doi.org/10.1016/j.sleep.2021.03.001.
[13] Russell GS, Eriksen KJ, Poolman P, et al. Geodesic photogrammetry for localizing sensor positions in dense-array EEG. Clin Neurophysiol 2005;116(5):1130–40. https://doi.org/10.1016/j.clinph.2004.12.022.
[14] Gabriel S, Lau RW, Gabriel C. The dielectric properties of biological tissues: II. Measurements in the frequency range 10 Hz to 20 GHz. Phys Med Biol 1996;41:2251–69.
[15] Oostendorp TFF, Delbeke J, Stegeman DFF. The conductivity of the human skull: results of in vivo and in vitro measurements. IEEE Trans Biomed Eng 2000;47:1487–92.
[16] Goncalves SI, de Munck JC, Verbunt JPA, et al. In vivo measurement of the brain and skull resistivities using an EIT-based method and realistic models for the head. IEEE Trans Biomed Eng 2003;50:754–67. https://doi.org/10.1109/TBME.2003.812164.
[17] Baumann SB, Wozny DR, Kelly SK, et al. The electrical conductivity of human cerebrospinal fluid at body temperature. IEEE Trans Biomed Eng 1997;44:220–3.
[18] Lindenblatt G, Silny J. A model of the electrical volume conductor in the region of the eye in the ELF range. Phys Med Biol 2001;46:3051–9.
[19] Steriade M. The corticothalamic system in sleep. Front Biosci 2003;8:d878–99.
[20] Junghofer M, Elbert T, Tucker DM, et al. The polar average reference effect: a bias in estimating the head surface integral in EEG recording. Clin Neurophysiol 1999;110(6):1149–55.
[21] Malmivuo J, Plonsey R. Bioelectromagnetism. New York, NY: Oxford University Press; 1995.
[22] Nunez PL, Srinivasan R. Electrical fields of the brain: neurophysics of EEG. New York, NY: Oxford University Press; 2005.
[23] Timofeev I, Chauvette S. Thalamocortical oscillations: local control of EEG slow waves. Curr Top Med Chem 2011;11(19):2457–71.
[24] Helfrich RF, Mander BA, Jagust WJ, et al. Old brains come uncoupled in sleep: slow wave-spindle synchrony, brain atrophy, and forgetting. Neuron 2018;97(1):221–30. https://doi.org/10.1016/j.neuron.2017.11.020. e4.
[25] Marshall L, Molle M, Hallschmid M, et al. Transcranial direct current stimulation during sleep improves declarative memory. J Neurosci 2004;24(44):9985.
[26] Marshall L, Helgadóttir H, Mölle M, et al. Boosting slow oscillations during sleep potentiates memory. Nature 2006;444(7119):610–3. https://doi.org/10.1038/nature05278.
[27] Achermann P, Finelli LA, Borbély AA. Unihemispheric enhancement of delta power in human frontal sleep EEG by prolonged wakefulness. Brain Res 2001;913(2):220–3.
[28] Sanchez-Vives MV, Massimini M, Mattia M. Shaping the default activity pattern of the cortical network. Neuron 2017;94(5):993–1001.
[29] Mesulam MM. Behavioral neuroanatomy: large-scale networks, association, cortex, frontal syndromes, the limbic system, and hemispheric specializations. In: Principles of behavioral and cognitive neurology. Oxford: Oxford University Press; 2000.
[30] Pandya DN, Barnes CL. In: Perecman E, editor. Architecture and connections of the frontal lobe. New York, NY: The IRBN Press; 1987.
[31] Pandya DN, Seltzer B. Association areas of the cerebral cortex. Trends Neural Sci 1982;5:386–90.
[32] Pandya DN, Seltzer B, Petrides M, et al. Cerebral cortex: architecture, connections, and the dual origin concept. New York, NY: Oxford University Press; 2015.
[33] Amaral DG, Price JL, Pitkanen A, et al. In: Aggleton JP, editor. Anatomical organization of the primate amygdaloid complex. New York, NY: John Wiley & Sons; 1992.
[34] Carmichael ST, Price JL. Limbic connections of the orbital and medial prefrontal cortex in macaque monkeys. J Comp Neurol 1995;363(4):615–41.
[35] Narikiyo K, Mizuguchi R, Ajima A, et al. The claustrum coordinates cortical slow-wave activity. Nat Neurosci 2020;23(6):741–53.
[36] Jackson J, Smith JB, Lee AK. The anatomy and physiology of claustrum-cortex interactions. Annu Rev Neurosci 2020;43.
[37] Tucker DM, Luu P. Cognition and neural development. New York, NY: Oxford University Press; 2012.
[38] Butler AB, Molnar Z. Development and evolution of the collopallium in amniotes: a new hypothesis of field homology. Brain Res Bull 2002;57:475–9.
[39] Bernardi G, Betta M, Ricciardi E, et al. Regional delta waves in human rapid eye movement sleep. J Neurosci 2019;39(14):2686–97.
[40] von Ellenrieder N, Gotman J, Zelmann R, et al. How the human brain sleeps: direct cortical recordings of normal brain activity. Ann Neurol 2020;87(2):289–301.